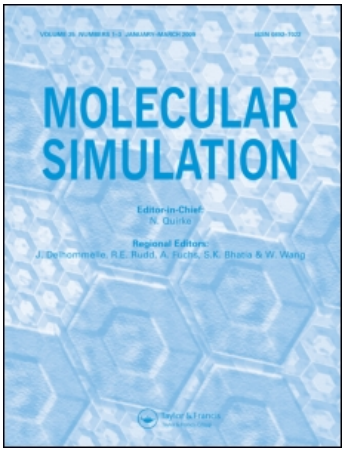

Molecular Simulation
Publication details, including instructions for authors and subscription information:
http://www.informaworld.com/smpp/title~content=t713644482

Brownian Dynamics Computer Simulations of Quenched Lennard-Jones-like Fluids: I Morphology and Local Structural Evolution

J. F. M. Lodge[ab]; D. M. Heyes[a]
[a] Department of Chemistry, University of Surrey, Guildford, United Kingdom [b] Colburn Laboratory, Department of Chemical Engineering, University of Delaware, Newark, Delaware, USA

To cite this Article Lodge, J. F. M. and Heyes, D. M.(1999) 'Brownian Dynamics Computer Simulations of Quenched Lennard-Jones-like Fluids: I Morphology and Local Structural Evolution', Molecular Simulation, 23: 3, 203 — 241
To link to this Article: DOI: 10.1080/08927029908022123
URL: http://dx.doi.org/10.1080/08927029908022123

Molecular Simulation, 1999, Vol. 23, pp. 203–241
Reprints available directly from the publisher
Photocopying permitted by license only

BROWNIAN DYNAMICS COMPUTER SIMULATIONS OF QUENCHED LENNARD-JONES-LIKE FLUIDS: I MORPHOLOGY AND LOCAL STRUCTURAL EVOLUTION

J. F. M. LODGE* and D. M. HEYES†

Department of Chemistry, University of Surrey, Guildford, GU2 5XH, United Kingdom

(Received July 1999; accepted August 1999)

The structural characteristics during phase separation of a model colloidal system were investigated using Brownian dynamics simulation. The structures that formed were analysed using the radial distribution function and structure factor in separate time periods after the quench. The data were interpreted in terms of scale-invariancy and density inhomogeneities. The systems, which consisted of a gas-like phase and dense liquid or solid-like regions, developed with a highly interconnected morphology during the simulations. The aggregate morphology was sensitive to the range of the attractive part of the potential and the position in the phase diagram after the quench. The long-range 12:6 potential induced compact structures with thick filaments, whereas the systems generated using the shorter-ranged 24:12 and 36:18 potentials persisted in a more diffuse network and also evolved more slowly with time. The fractal dimensions were quite high, typically close to 3. The 24:12 and 36:18 potential systems developed regions of local crystalline order which formed contemporaneously with the more global morphological changes. In contrast, at low temperatures the particles of the longer-range 12:6 potential became trapped in glass-like states during the course of the morphological changes in the system. The value of the characteristic lengthscale with time exponent, α, was found to be dependent on the temperature, density and interaction potential and therefore cannot be described as 'universal'.

Keywords: Colloidal system; Brownian dynamics; quenched fluids

*Present address: Colburn Laboratory, Department of Chemical Engineering, University of Delaware, Newark, Delaware 19716, USA.
†Corresponding author.

1. INTRODUCTION

The term 'colloidal' refers to a physical state containing small particles of between 1 nm and 1 μm in diameter, in a background or 'dispersion' medium of much smaller particles. A variety of different colloidal types exist depending on the phases of the two constituents. This work concentrates on the behaviour of 'sols', which are solid particles dispersed in a liquid dispersion medium. Their colloidal chemistry is of significant practical importance, as these materials form the basis of a wide range of consumer products such as cosmetics, foodstuffs, paint and pharmaceuticals. Also many industrial processes rely heavily on colloidal phenomena, for example sewage treatment, paper-making and oil well drilling. These numerous applications have been in no small part responsible for the experimental and theoretical interest in colloidal systems in recent years. The existence of matter in the colloidal state may be either desirable or undesirable, depending on the application of the material. It is therefore important to understand the various colloidal states and the factors that influence their formation and physical properties.

Owing to the complexity of colloidal systems, they often cannot be treated at the same level of molecular detail as is possible for simpler molecular systems (although nanocolloids have now been treated now by Molecular Dynamics a number of times [1]). The wide range of time and lengthscales associated with the two components is an inherent feature of colloidal systems, and presents the major challenge to computational and theoretical treatments. On the experimental side, colloidal liquids can offer advantages over simple molecular systems (*e.g.*, argon or water) since colloidal particles are much larger than simple molecules (ca. 1 – 1000 nm in diameter as opposed to 0.1 – 1 nm, respectively). Their diffusivity is significantly lower, and phenomena such as phase separation, the subject of interest here, occurs on more readily observable timescales, in contrast to the very fast times characteristic of simple atomic systems ($\sim ps$ to ns). Also, since the lengthscales are typically in the optical wavelength region, colloidal liquids can be probed for structural arrangement and interactions using a range of laser optical techniques such as laser light scattering, confocal optical microscopy and optical 'tweezers'.

A characteristic feature of colloidal particles that distinguishes them from simpler molecular systems is the presence of solvent-derived stochastic forces that lead to 'Brownian motion' of the particles. The importance of these forces for colloidal species is a consequence of the particle size.

Colloidal particles are large enough to be distinguished from the solvent but small enough to be displaced by the density fluctuations in the solvent, resulting in the apparent random and irregular motion of the particles. A stable colloidal liquid would not exist without these Brownian forces, as they maintain the particles in a suspended state. One can consider the Brownian forces as the source of equipartition of kinetic energy between solvent molecules and colloidal particles. A system of colloidal particles in a fluid displays equilibrium phases equivalent to simple molecular systems with the same pair potential at the same points on the reduced phase diagram. At very low concentrations the particles are in a gas-like state. At higher concentrations, fluid or liquid-like states exist which possess some short-range order, highly ordered crystal-like states can form and even metastable glass-like-states. In fact, in many ways, colloidal dispersions exhibit a much more interesting and useful range of structural and morphological states than simple molecular systems because of the existence of long-lived metastable and unstable states. In simple molecular systems these are too short-lived to be of practical value.

The phase diagrams of colloidal liquids can be adjusted by 'tuning' the interaction potential. Colloidal particles are inherently thermodynamically unstable to the coagulated state owing to the very large surface area to volume ratio of the dispersed particles. The colloidal particles can be kinetically stabilised against the van der Waals attractive forces by adsorbed or grafted polymers, which provide a steric or entropic stabilisation to prevent the particles from approaching within the strongly attractive potential range ('primary minimum'). Alternatively, particles in an aqueous solution can be charged, which creates an electrical double layer repulsion between the particles. The stabilising effect can be removed, or an effective attraction between the particles added, to cause the particles to aggregate. Aggregation can be induced in aqueous charge-stabilised systems by changing the concentration of salt to neutralise the stabilising charge. Alternatively, polymers can be added which can preferentially attach themselves to the particles, thus causing aggregation by a bridging mechanism. Systems can also be destabilised by the addition of free polymer that results in an osmotic-pressure derived attraction between colloidal particles. This is known as the 'depletion' effect. The effective inter-particle attraction is proportional to the osmotic pressure of the polymer solution and can be quite large, in excess of 40 k_BT. Aggregation in a model system of particles possessing an attractive part to the interaction potential can be induced by lowering the temperature of the system, which is thermodynamically equivalent to making the

colloidal particles more attractive in real systems. The ratio of the temperature to the depth of the attractive interaction potential well between the colloidal particles is the important quantity.

When a system is quenched from the one phase region down into the two phase region, the system evolves to a state consisting of two coexisting phases. Phase separation occurs through the temporal evolution of spatial fluctuations by two mechanisms. Instability to short wavelength fluctuations results in a nucleation and growth type of separation, whereas an instability to long wavelength fluctuations leads to phase separation through a spinodal decomposition mechanism. Spinodal decomposition is associated with an interconnected morphology that can, in principle, be identified with the percolating structure often found in gels. Of course, an interconnected network will not necessarily provide sufficient rigidity to confer gel-like rheology on the system, so the occurrence of such a network requires some careful physical characterisation. A similar interconnected morphology, however, can also be obtained from the superposition of clusters formed at some stage after nucleation, so such a structure does not necessarily distinguish the phase separation mechanism [2].

The morphology of colloidal aggregates can vary from loose liquid-like flocs to more solid-like amorphous or crystalline clusters, depending on the temperature of the system and on the interaction forces between the particles [3]. A colloidal gel is a flocculated state in which a continuous network of particles filling the container is formed before settling can occur, as is shown schematically in Figure 1. The network structure consists of key stress bearing 'backbone' paths of particles, with side branches that do not support the stress and are therefore largely redundant rheologically.

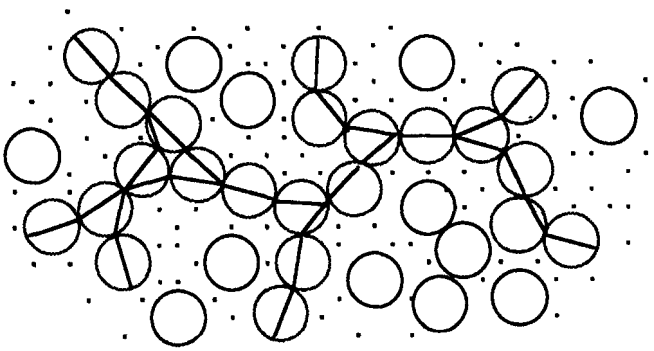

FIGURE 1 Diagram of aggregated particles forming a system spanning colloidal gel showing the key 'backbone' particles of the gel.

The high connectivity between the particles and a divergence in the average cluster size near the gel point gives rise to a high dispersion viscosity at low shear rates and a slowing down of structural relaxation processes with the appearance of an apparent yield stress. Stress time autocorrelation functions in a gelling system develop a power law decay at short times, terminating in a stretched exponential [4, 5]. The power law region is expected to extend to longer times as the gel point is approached. The gel point is characterised by a divergence in viscosity before the gel point and an increase in the elastic modulus, G, after the gel point.

Gels are typically soft and elastic with a relatively low percentage of solid matter (sometimes as low as several percent). The specific properties of an individual gel depend largely on the strength and type of the interparticle interactions. In the case of particles forming permanent chemical bonds, such as cross-linking polymers, the gels are stable and the sol-gel transition corresponds to a transition from a liquid to a permanent solid network. However, gels can also be formed from particles with reversible bonding characteristics. The gels formed in this case are thermodynamically unstable and have a finite lifetime with a tendency to collapse on quite short (*i.e.*, minute) timescales. These physical gels have relatively weak attractive interactions, typically between $2-10\,k_BT$. Aggregates may undergo extensive restructuring during formation and can be readily redispersed.

This work concentrates on the more weakly associating systems that do not form permanent bonds. The reversible bonding and low interaction strength can cause difficulty in the definition of a transient gel, since gel-like properties are weak and the systems are typically viscous. The assumption of the existence of a low yield stress has not yet been confirmed experimentally. The presence of a percolating network is not necessarily enough to confer gel-like rheology, since for reversible interactions the particles forming the network can be quite mobile and in this case the network will have minimal stress bearing capacity. One of the main objectives of the present work was to discover the structural aspects of the phase separation of potentially gel forming colloidal particles – prior to a rheological characterisation. In the next section, the details of the computational model are described.

2. MODEL AND COMPUTATIONAL DETAILS

The model system consisted of N spherical particles of diameter σ, contained in a cubic simulation cell of volume V. The volume fraction, ϕ, for this

system is,

$$\phi = \frac{\pi}{6}\frac{N\sigma^3}{V} \tag{1}$$

The volume fractions used in the simulations were $\phi = 0.05$, 0.10, 0.16 and 0.20. Interactions between model colloidal particles were represented by a generalised Lennard-Jones *m-n* pair potential,

$$U(r) = A\varepsilon\left[\left(\frac{\sigma}{r}\right)^m - \left(\frac{\sigma}{r}\right)^n\right] \tag{2}$$

where r is the inter-particle centre-to-centre separation distance, σ is the particle 'diameter', and A is the normalisation factor to ensure that $-\varepsilon$ is the minimum potential energy in the potential. The interaction was truncated at 2.5σ, and in this work $m = 2n$ and therefore $A = 4$ in each case. The minimum in the potential, r_m, is at a separation of $2^{1/n}\sigma$ with $m = 2n$, which therefore is displaced to smaller separations as m increases. The values of m chosen for the simulations were 12, 24 and 36. The 12:6, 24:12 and 36:18 potentials are compared in Figure 2. Along this series the attractive part of the potential becomes shorter ranged. The range of the interaction potential influences the phase diagram and the rheology of the colloidal system. The long-ranged Lennard-Jones12:6 potential is probably the only example that has a gas–liquid equilibrium. This leaves vapour–solid as the two low temperature co-existing phases for the other two.

The state points that were considered in our simulations were at reduced temperatures of $T^* = k_BT/\varepsilon = 0.01$, 0.05, 0.3 and 0.5, for all potentials and additionally at $T^* = 0.7$ and 0.9 for the 12:6 potential (we will omit

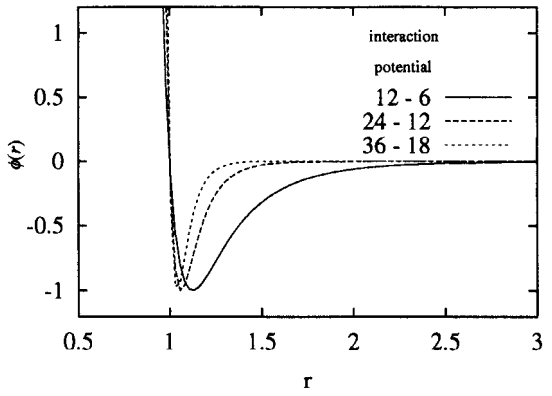

FIGURE 2 Comparison of the *n:m* potentials used in the simulations.

the * henceforth). At $T = 0.01-0.5$, the phase points are all in the two phase vapour–solid co-existence region, however for the 36:18 potential, the $T = 0.5$ and $\phi = 0.05$ state point lies just inside the one phase region [6]. For the 12:6 potential the critical and triple point temperatures are 1.32 and 0.69 respectively [7]. The phase points at $T = 0.7$ and 0.9 with this potential are therefore also within the vapour–liquid coexistence region.

The Brownian Dynamics, BD, technique devised by Ermak was used to generate the trajectories of the interacting model colloidal particles by numerically integrating the position Langevin equation in finite time steps using a first order scheme [9]. The Brownian forces are chosen randomly from a Gaussian probability distribution with a zero average. The mean square displacement is $6k_BT\Delta t/\zeta_0$, where Δt is the timestep used in the simulation and ζ_0 is the infinite dilution coefficient of friction. The self-diffusion coefficient at infinite dilution is $D_0 = k_BT/\zeta_0$. The thermodynamic properties are given in units of σ for length and ε for energy. The units of time are those traditionally chosen for colloidal liquids, a^2/D_0, where a is the radius of the particle ($=\sigma/2$) and D_0 is the self-diffusion coefficient of the colloidal particles in the infinite dilution limit. As the value of D_0 is given by, $D_0 = k_BT/\zeta_0$, therefore in reduced units if we define $\zeta_0^* = 1$ then $D_0^* = T^*$.

An equilibrated high temperature system at $T = 2.0$ was 'quenched' to a low temperature phase point in a single time step, representing an essentially instantaneous quench. The initial homogeneous system phase at the low temperature eventually separated into the two coexisting phases. The quench procedure was repeated five times from statistically independent state points to improve the statistical averaging. A typical system size consisted of 864 colloidal particles with a total simulation length of $81.9\,a^2/D_0$. Some larger systems of 4000 particles were used to establish the N-dependence of the results. A total of 25 time intervals or segments of duration $\tau_{\text{int}} = 3.2\,a^2/D_0$ were used to follow the time evolution of the system properties towards the thermodynamic equilibrium.

3. RESULTS AND DISCUSSION

3.1. Configuration Images

The structural evolution of phase separating systems forms the basis of many theoretical treatments. Structure in experimental systems is often difficult to follow accurately, relying on microscopy for direct observation and scattering techniques for more quantitative statistical details. A visual

representation created from the particle co-ordinates produced during the simulations shows the initial homogeneous system separating into regions of widely varying density. Examples of the final structure at $t = 81.92\ a^2/D_0$ for several volume fractions at the reduced temperature, $T = 0.3$ are shown in Figure 3 for the 12:6 potential and in Figure 4 for the 36:18 potential, using 864 particles in each case. In all of the systems that show significant phase separation, aggregation of the particles is apparent at the earliest times. The 12:6 systems tend to adopt a concave surface morphology at higher volume fractions. The tendency of the surfaces to adopt this concave morphology seems to be a characteristic feature of the longer-ranged potentials. The thin 'necks' between the dense 'blobs' can presumably sustain a significant elastic stress if there is a long-range attractive potential conferring cohesion to the assembly of particles.

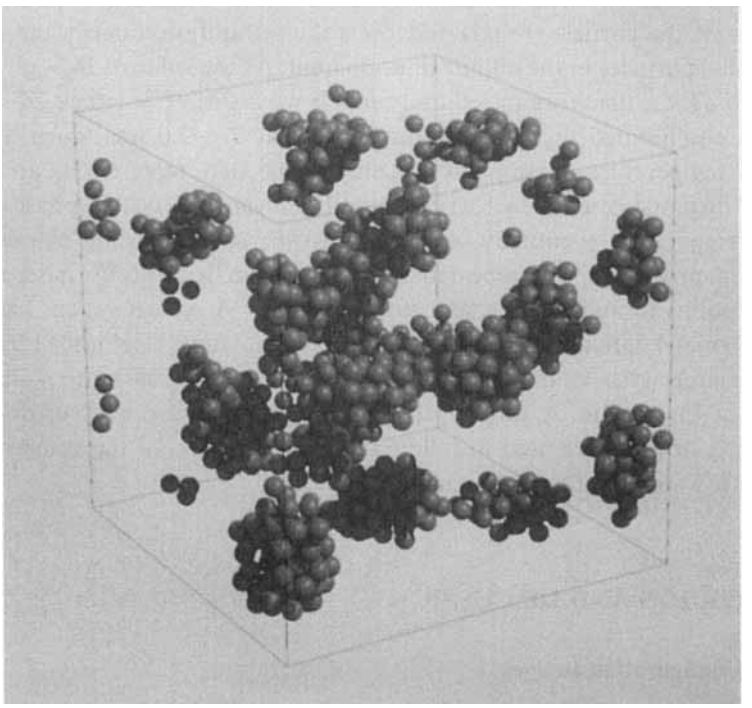

FIGURE 3 Snapshots showing the temporal evolution of structure in a system of 864 particles at various volume fractions and $T = 0.3$ for the 12:6 interaction potential (a) $\phi = 0.05$ (b) $\phi = 0.10$ (c) $\phi = 0.16$ and (d) $\phi = 0.20$. Snapshots shown are taken at the final simulation step at $t = 81.92\ a^2/D_0$. The spheres represent 1σ and are drawn to scale in relation to the simulation box. (See Color Plate I).

(b) $\phi = 0.10$

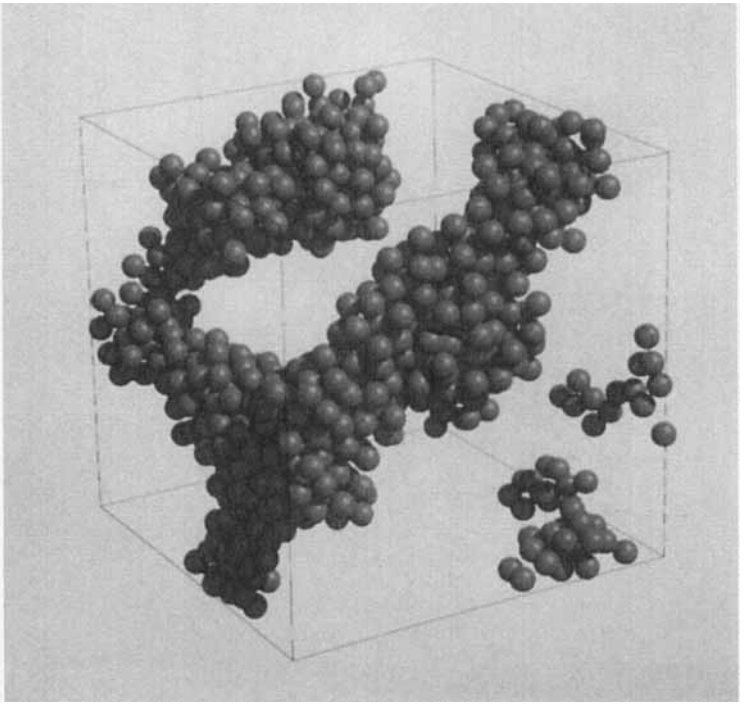

FIGURE 3 (Continued).

3.2. Radial Distribution Functions

In general, after a temperature quench, the pair distribution functions, $g(r)$, show an increase in the intensity of the first peak and growth with time of peaks at longer range. An example of this typical behaviour is given in Figure 5, which shows the results of a simulation using a 12–6 potential at $\phi = 0.16$ and $T = 0.7$. The first peak displays quite a dramatic growth in intensity during the phase separation which is a result of the clustering of particles. Peaks also develop at longer distances, again increasing in intensity with time, reflecting the increasing size of the dense clusters. The single peaks suggest the formation of a dense liquid phase which points to a fluid–fluid phase separation.

The intensity of the peaks increases with decreasing temperature, possibly because at lower temperatures the mean square random displacements are smaller and the attraction between particles can then lead to more compact

(c) $\phi = 0.16$

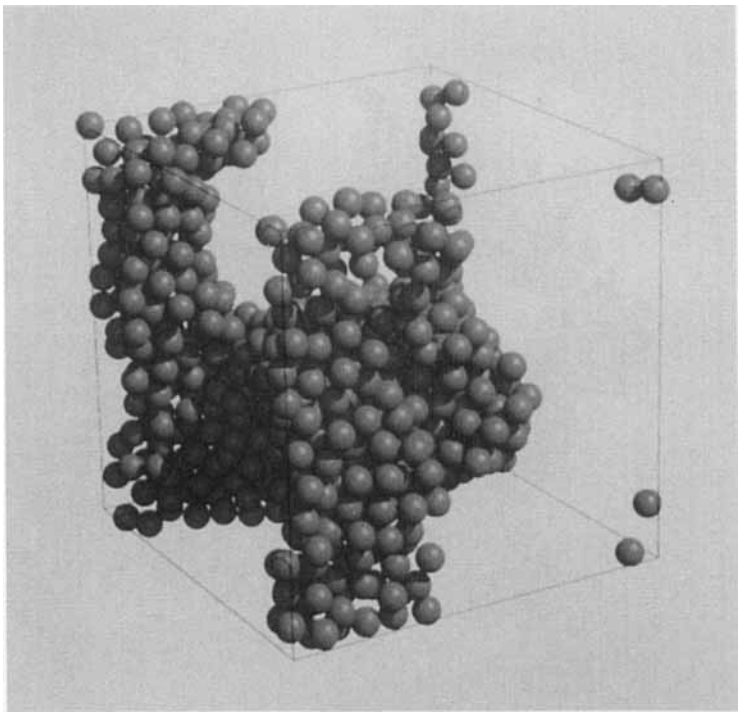

FIGURE 3 (Continued).

clustering and increase in the number of associations on that lengthscale. The intensity also increases with decreasing volume fraction, which is something of an 'artefact' of the larger difference between the local density in the cluster and the average density of particles in the system for these lower volume fraction systems. The increase in intensity of these peaks is observed for all of the interaction potentials.

The 24:12 and 36:18 interaction potential systems showed a tendency to form local face-centred cubic (FCC) order, whereas the 12:6 potential systems had a greater tendency to become 'trapped' in an amorphous or glassy structure. Local 'crystallisation' of the particles is reflected in the $g(r)$ as an additional peak at $r \approx \sqrt{2}\sigma$. An example of this behaviour is shown in Figure 6(a) for a 24:12 potential system at $\phi = 0.20$ and $T = 0.3$. The first non-integer peak appears at 1.49σ. Some of the lower temperature higher volume fraction systems show signs of the formation of an amorphous structure. For amorphous systems such as glasses the second peak

(d) $\phi = 0.20$

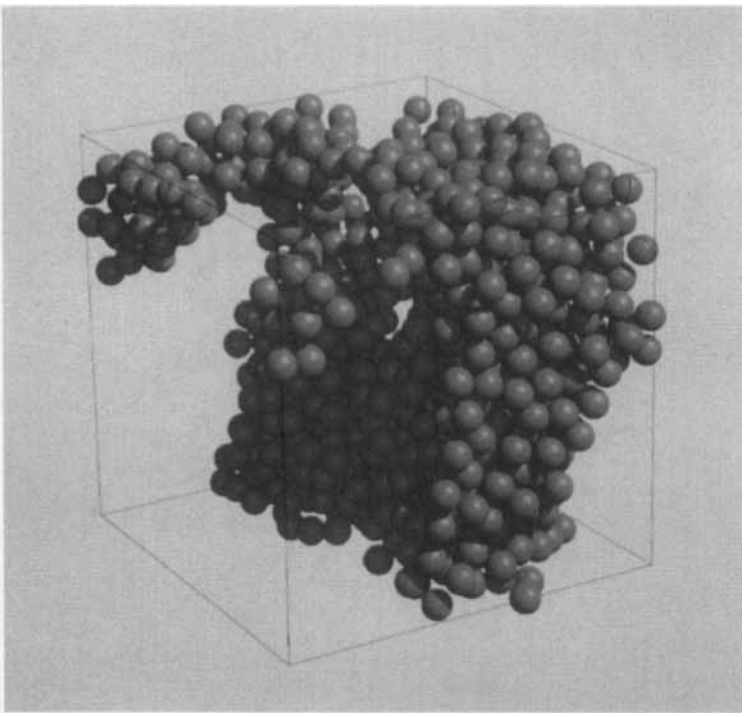

FIGURE 3 (Continued).

in the radial distribution function is split characteristically into an overlapping double peak. These features are displayed well by the 12:6 systems, for example at $\phi = 0.2$ and $T = 0.3$, the radial distribution functions for which are shown in Figure 6(b). The particles consolidate into structures with well-defined geometries that are reflected in the split peaks. The non-equilibrium structures in the packing of the particles are probably due to the appearance of two dominating three-particle relative dispositions in the local packing that are illustrated schematically in Figure 7. Therefore the longer-range potentials have the potential to become trapped in glassy-like states in the condensed parts of the system.

The larger sphere of influence of the 12:6 potential probably increases the activation energy barrier in the path from a random to an ordered structure when compared with the behaviour of the shorter-range potentials. This is possibly because particles from the second and even the third co-ordination shells of near neighbours are involved in a more highly co-operative

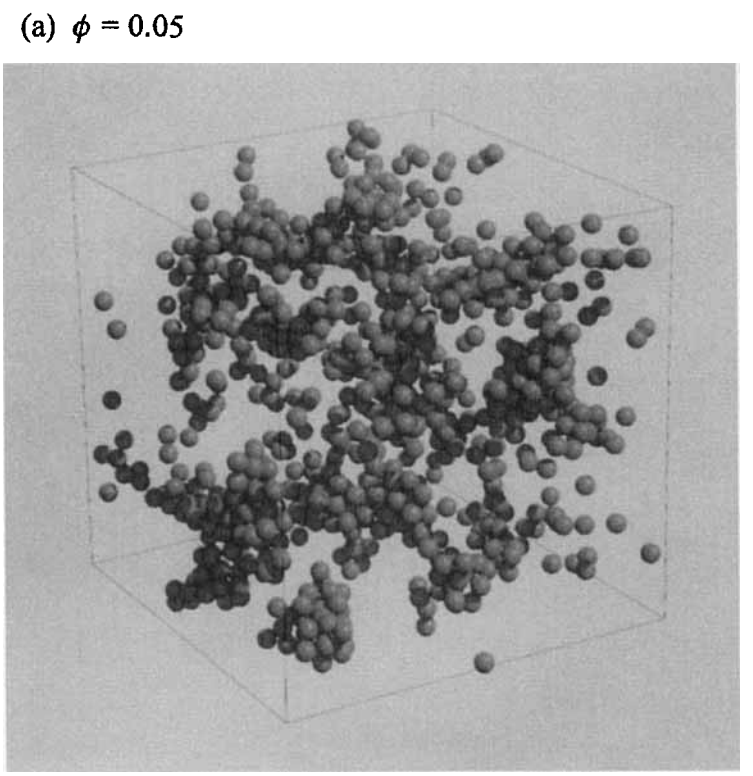

FIGURE 4 As for Figure 3 except the 36:18 potential was used. (See Color Plate II).

rearrangement process. The free energy landscape is rougher and with more and deeper minima within which the system can become trapped. Therefore at low temperatures, the systems can become trapped in these metastable amorphous states which do not relax into their equilibrium crystal arrangements during the timescale of the major condensation and morphological changes observed in the 12:6 system simulations.

The radial distribution functions also provide insights into the long-range morphological changes taking place in the model quenched colloidal liquids. Along with the increasing local structure at long times there is an accompanying dip in the pair distribution function below $g(r) = 1$ at large separations. This 'depletion zone' which appears soon after the peaks at shorter distances is a characteristic feature of phase separating systems. The systems become increasingly inhomogeneous with time and surrounding the dense regions there are 'compensating' regions of a lower than average density. It is reasonable to assume that the distance to the middle of the

(b) $\phi = 0.10$

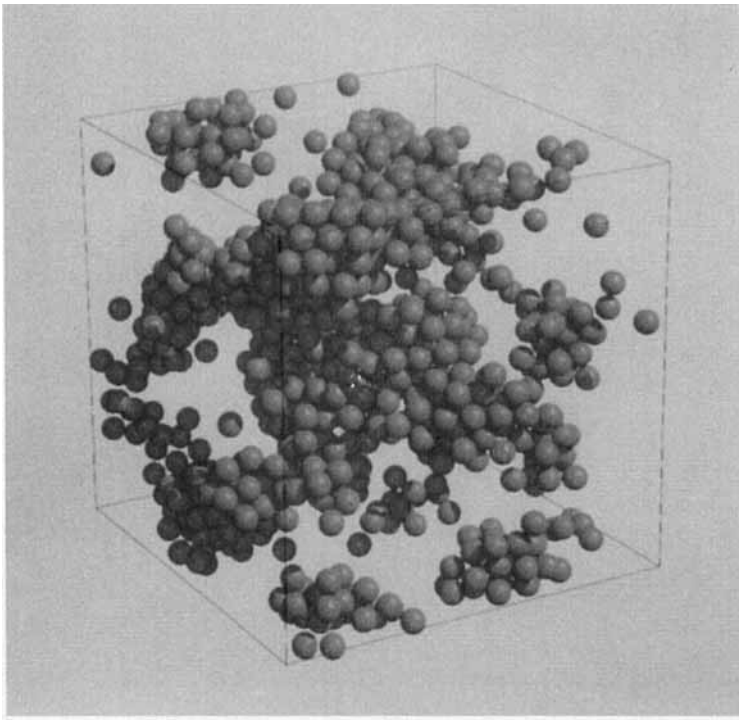

FIGURE 4 (Continued).

dip is approximately half the inter-cluster separation, and is therefore the position of the minimum in this dip is a measure of the characteristic length-scale of the systems. (This can also be estimated from the position of the small angle scattering peak in the structure factor, which is discussed in more detail below.) As the clusters increase in size with time, the minimum in $g(r)$ moves to longer distances. An example of this behaviour is given in Figure 8 for an 12:6 $\phi = 0.16$ and $T = 0.7$ system. At early times (*i.e.*, $t \approx 10$) the whole of the dip is visible on the plot, and $g(r)$ returns to unity within the length of half of the box. However, at intermediate times (*i.e.*, $t \approx 36$), as the cluster size increases the dip moves to greater distances and the return of $g(r)$ to unity is not possible within the scale of the simulation box. This gives a good illustration of the importance of performing such simulations for a series of system sizes. Eventually at long enough times the length-scale of the structures that develop will be comparable with the dimensions

(c) $\phi = 0.16$

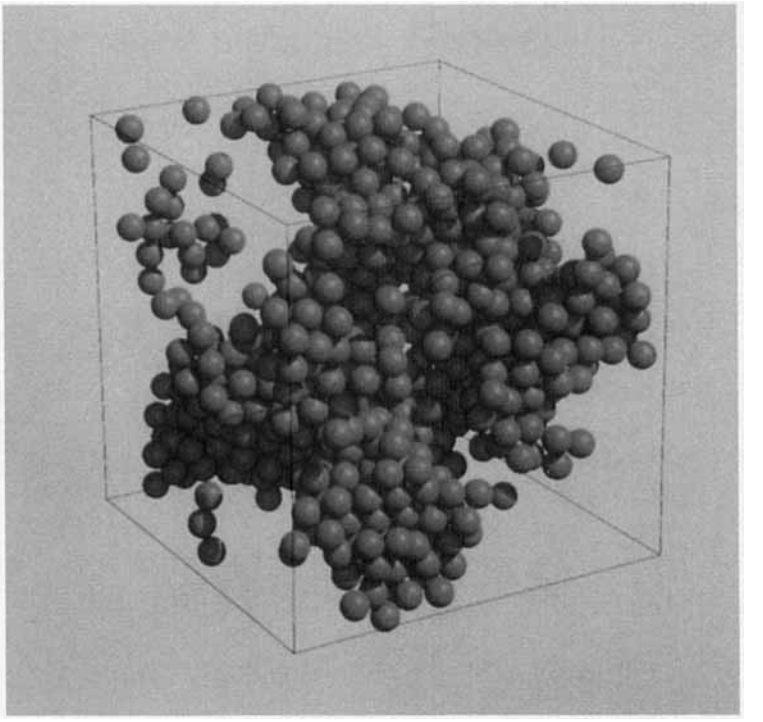

FIGURE 4 (Continued).

of the simulation cell. The advantage of increasing the system size is that the phase separation can be followed out to longer times before the finite-size effects start to dominate and distort the system's evolution.

3.3. Structure Factors

The long range structure was also characterised during the phase coarsening after the quench through the structure factor, $S(k)$, which is derived from the pair distribution function, $g(r)$, by the Fourier transformation [7],

$$S(k) = 1 + 4\pi\rho \int_0^\infty (g(r) - 1) r^2 \frac{\sin(kr)}{kr} dr \tag{3}$$

This function is particularly suitable for highlighting the development of long-range order in the system that cannot be perceived so readily in $g(r)$.

(d) $\phi = 0.20$

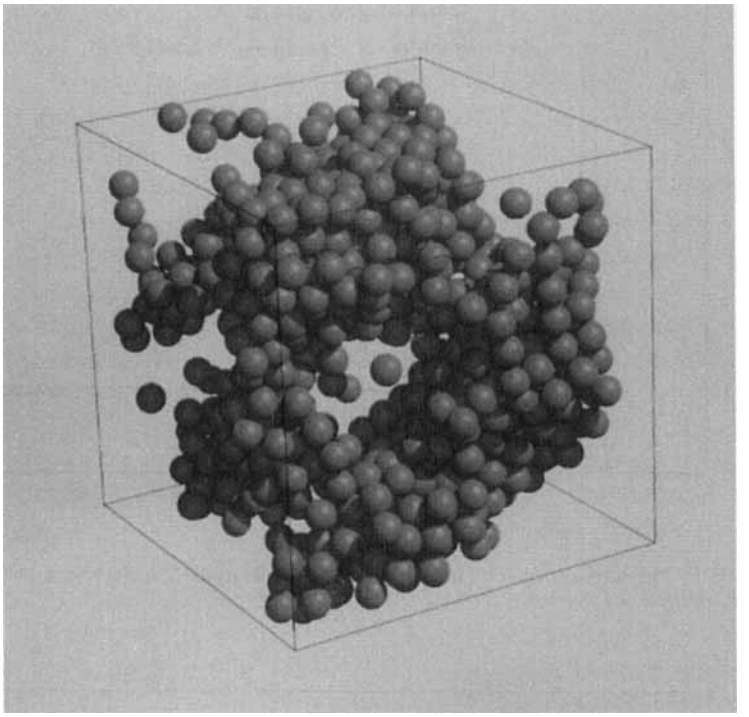

FIGURE 4 (Continued).

The structure factors in most of the systems studied in this work developed a peak at low wavevector ($k = k_m \approx 1$) immediately or soon after the quench. The appearance of a peak at low wavevector is a signature of phase separation and does not occur in equilibrium single phase states. Since this peak originates from long wavelength correlations, it grows in height with the progressive aggregation of particles into clusters and therefore reflects the range and amount of long-range structure in the system. The position of this peak gives the characteristic lengthscale of the system ($\approx 2\pi/k_m$), which can give an indication of the intercluster distance or of the cluster size since in spinodal decomposition the two domain sizes are equivalent.

The time dependent behaviour of the small angle scattering peak can be used to distinguish the phase separation mechanism. Typically, for the spinodal decompostion mechanism, this new low-k peak grows in height and moves to lower wavevector with time. An example of such a behaviour is given in Figure 9 for a $\phi = 0.1$ and $T = 0.7$ 12:6 system. A number of the

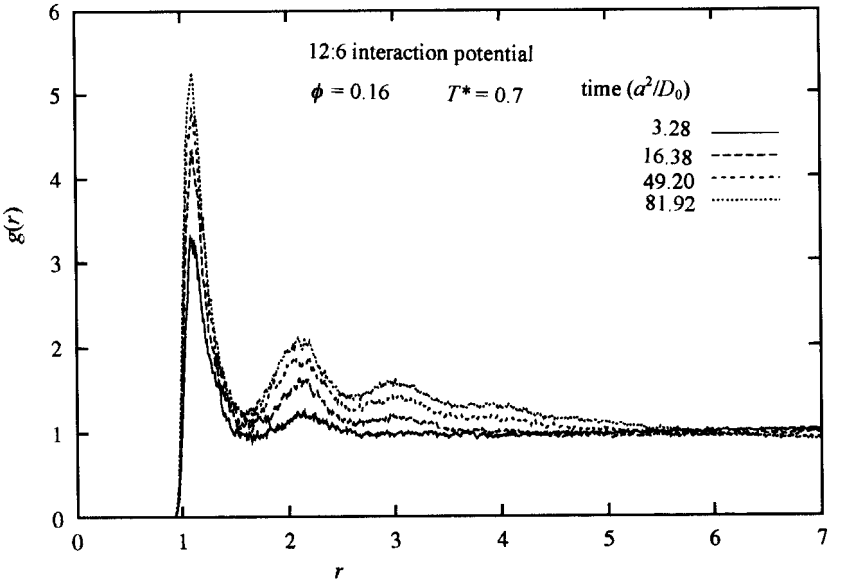

FIGURE 5 The radial distribution function at various times from the quench for a 12:6 potential with $\phi = 0.16$ and $T = 0.7$.

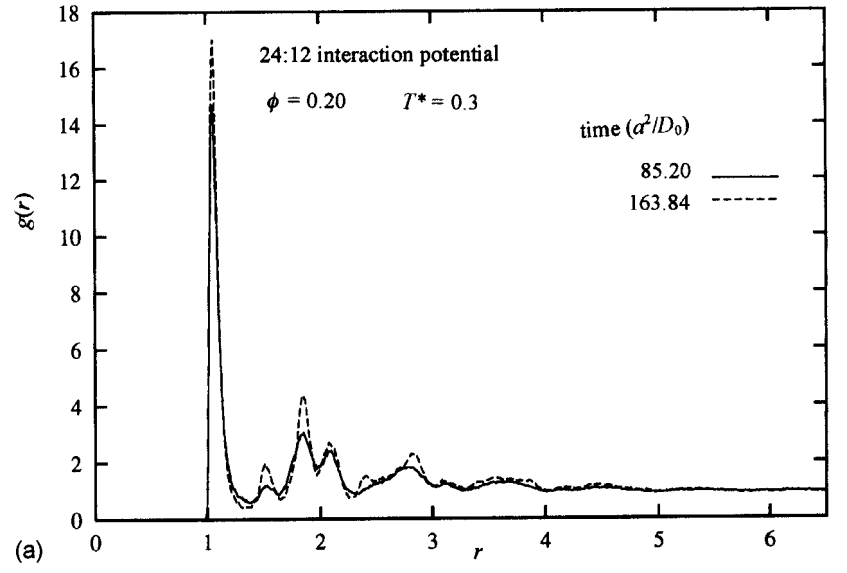

FIGURE 6 The radial distribution function at various times from the quench at $\phi = 0.20$ and $T = 0.3$ (a) for the 24:12 potential showing the evolution of a degree of crystallinity in the structure (b) for the 12:6 potential (amorphous/glassy).

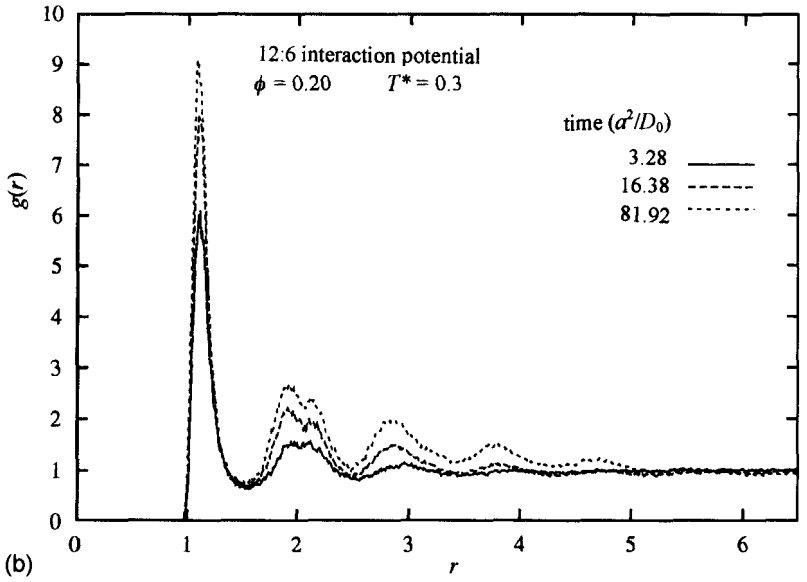

FIGURE 6 (Continued).

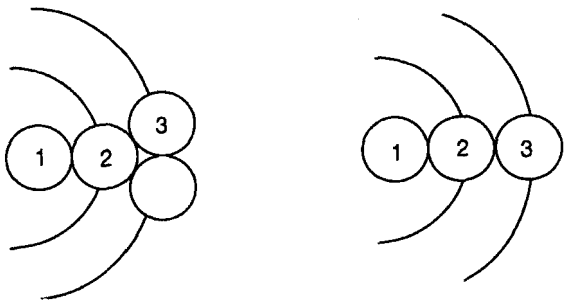

FIGURE 7 Diagram of two local packing arrangements of spherical particles giving rise to the split second peak in the radial distribution function.

simulated systems, mainly those which also display metastable behaviour (through a lack of peak growth) in the pair distribution functions, did not develop a well-defined peak for some time. There is some evidence from our simulations in the metastable region of a very low intensity peak that did not grow significantly in intensity. In metastable systems, clusters appear *via* an activated nucleation and growth mechanism, leading to the appearance of a weak low k-peak reflecting intraparticle and interparticle correlations. This peak is of such low intensity that it would probably not be

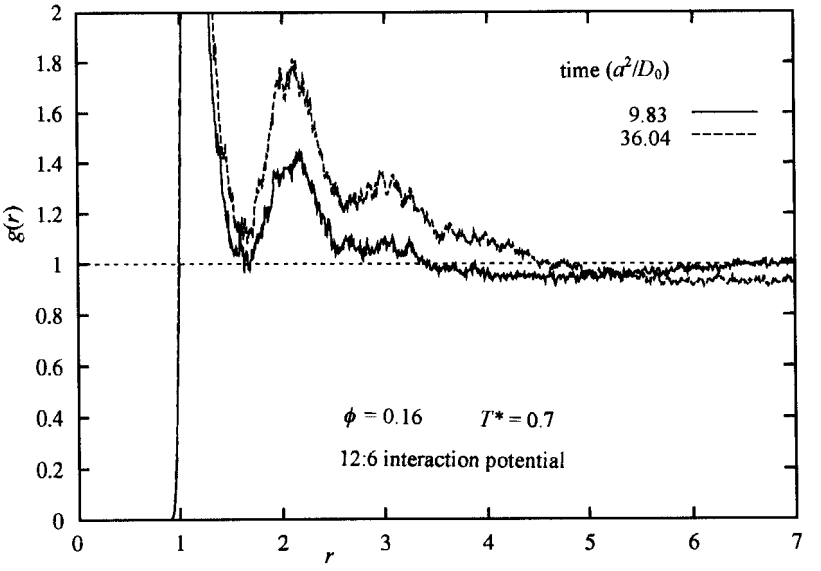

FIGURE 8 Radial distribution functions for the 12:6 potential system at $\phi = 0.16$ and $T = 0.7$ at two times late in the phase separation process.

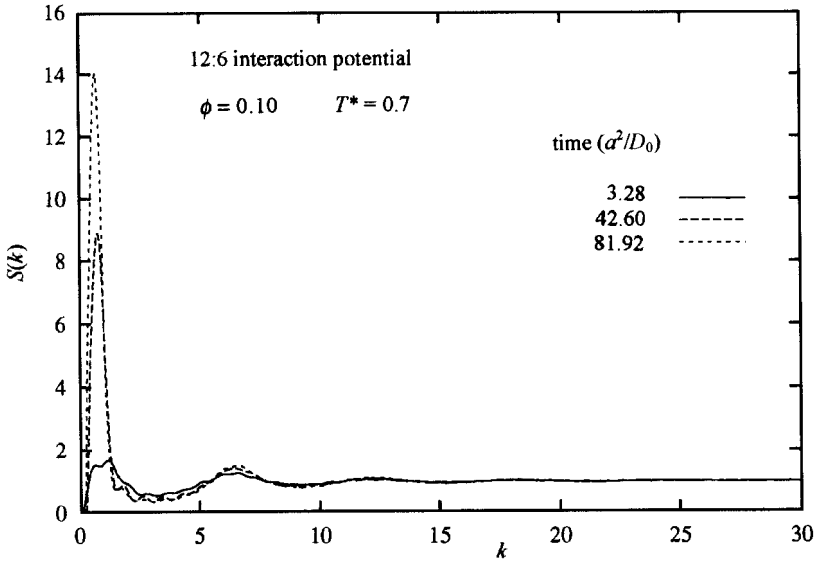

FIGURE 9 The time evolution of the structure factor, $S(k)$, for a 12:6 potential system with $N = 864$ particles and at $\phi = 0.10$ and $T = 0.7$.

discernible in light scattering experiments, which often report no peak in this part of the scattering regime for metastable systems. In light scattering work the absence of a peak for a period of time after the quench is termed 'latency'. This term is used here for systems that exhibited very low intensity peaks low-k peaks that did not increase in intensity. Other systems showed limited growth of the small angle scattering peak, although the peak did not display an immediate drift to lower wavevectors. This is termed 'position latency'. Latency is characteristic of systems separating *via* a nucleation and growth mechanism.

Most of the systems with the long-ranged 12–6 potential exhibit the classical behaviour of spinodal decomposition, namely the immediate appearance of a small angle scattering peak in the structure factor which gradually increased in intensity and decreased in wavenumber in time following the quench. The lowest volume fraction system, $\phi = 0.05$ at $T = 0.9$ showed full latency in both peak intensity and position after the initial appearance of a small peak. The system with the lowest volume fraction, $\phi = 0.05$, also showed position latency at $T = 0.7$, as did the $\phi = 0.10$ system at $T = 0.9$ (although the peak appeared immediately following the quench). The behaviour of these systems is indicative of phase separation by a nucleation and growth mechanism, which is expected in the metastable region of the phase diagram. The structure factor is more effective at bringing out long-range correlations than the pair distribution functions, which is why the tendency to nucleation and growth is manifest in the structure factor, but not always by the pair distribution functions, especially if the system is only marginally metastable.

As the interaction potential became shorter-ranged, the small angle scattering peak displayed increasing evidence of metastability reflecting the lowering of the two phase coexistence line in the phase diagram. For example, at $T = 0.5$ for the 12:6 potential, at all volume fractions an immediate phase separation was seen. In contrast, for the 24:12 potential the low volume fraction systems, $\phi = 0.05$ and 0.10, at a temperature of $T = 0.5$, showed some latency with little development of a small angle scattering peak. This implies that these two points are in the metastable region. The two highest volume fraction systems formed well-defined single peaks very early on in time. Although both showed some position latency at early times they later increased in intensity. For the shortest-range 36:18 potential, the higher temperature systems, $T = 0.5$, did not show significant peak development for any volume fraction. The highest volume fraction system, $\phi = 0.2$, showed a small increase, although this was not continuous and the intensity was still low. These systems are in fact very close to the

binodal coexistence line [6]. At the lower temperature of $T = 0.3$, systems for all potentials showed spinodal-like behaviour in the small angle scattering peak. A peak appeared immediately following the quench which increased in intensity and decreased in position gradually with time. The growth and movement of the peak was slower for the shorter-ranged potentials, again reflecting the closer position of this phase point to the metastable region.

In light scattering experiments after some time the small angle scattering peak has been observed to show no visible change in either intensity or position of the peak [9]. This has been ascribed to the formation of a transient gel in which the particles are effectively 'frozen' in their positions. After a certain length of time, the peak suddenly collapses leaving a forward scattering peak at zero wave vector. Although in this work some of the shorter-ranged potential systems exhibit a slowing of the phase separation, no completely 'frozen' system was observed and most of the systems phase separated continuously during the simulation. For all state points the peaks gradually increased in intensity and moved to lower wavenumbers during the simulation for all potentials with no indication of 'freezing', except perhaps at the phase point $T = 0.3$ and $\phi = 0.05$ for the 36:18 potential. This system did reach a point when the position of the peak no longer changed with time, although the intensity of the peak was still increasing. The peak position in this system was constant for a significant length of time, for the interval $t = 81.92 - 163.84\, a^2/D_0$.

The small angle scattering peak appears at higher wavevectors for shorter-ranged potentials. The 36–18 potential develops a peak at $k \approx 1.0$, whereas for the 12–6 systems, a peak typically appears at $k \approx 0.6$. Systems with long-ranged potentials aggregate at a faster rate than those with shorter-ranged potentials and it is likely that the early growth of the 12–6 potential was not captured by our sampling procedure owing to it not having a fine enough resolution in time.

The peak position, k_m is a measure of the inverse of the characteristic lengthscale of the system, the associated distance scale being $\approx 2\pi/k_m$. The dependence of the peak position on time characterises the key distance scale in the phase separation. A straight line in a log–log plot of the inverse of the peak position against time indicates a power law dependence of the characteristic lengthscale on time, $k_m^{-1} \propto t^{\alpha}$. There have been theoretical predictions for the value of α which is bounded at early times by $\alpha \leq 1/2$ [10]. The Lifshitz-Slyozov single particle diffusion mechanism [11] predicts 0.33, whereas an exponent of 0.2 comes from a cluster–cluster agglomeration mechanism [12, 13]. Late stage growth in percolating systems is often

characterised by an increase in α to a higher value of ≈ 1 which is caused by surface tension dominated phase separation [14]. Care must be exercised in deriving the exponent as the finite size of the model systems can cause a large increase in the apparent rate of phase separation described by the power law exponent of the peak position. However the peak position at short times before the rapid increase does not seem to be affected by these finite size effects. In higher volume fraction systems, therefore, only the early time data was used in calculating α, before finite size effects become apparent. The time at which finite size effects became evident depended on the volume fraction and the temperature.

Many of the systems with crossovers, latency or finite size effects demonstrate a gradual change in the value of the exponent with time so that the overall shape of k_m^{-1} against time is curved. For systems showing finite size effects, values of α were taken before any finite size effects had became apparent. For systems showing signs of position latency, exponents were taken from data at later times when the peak position began to decrease.

For most of the systems studied in this work, the characteristic length-scale, k_m^{-1}, increased with time as the phase separation progresses. A power law dependence on time was found, sometimes following latency, with early time exponents varying between 0.14 and 0.33, comparing quite well with experiment and theory. The value of the exponent was dependent on the temperature, density and interaction potential and therefore cannot be described as 'universal'.

The values for the growth exponent α for the 12:6 potential were dependent on the state point, and are shown in Table I. The high temperature and low volume fraction systems showed signs of latency. At $\phi = 0.05$ with $T = 0.9$ and 0.7, the peak showed no clear decrease in position with time, whilst at $\phi = 0.10$ at $T = 0.9$, a period of very slow decrease was followed by one of faster growth. The noise was significant during

TABLE I Behaviour of the first peak position in the structure factor, $k_m^{-1} \propto t^{\alpha}$, for the 12:6 potential. The values of α are for $T = 0.3$ taken at intermediate times. Any significantly different value after a crossover at later time is shown in brackets. The symbol, FS, indicates the occurrence of a continual decrease of the peak position to zero towards the end of the simulation, caused by finite size effects. The results marked with * are for the slightly smaller 256 particle systems. The uncertainty in each value is estimated to be ± 0.02

T/ϕ	0.05	0.10	0.16	0.20
0.9	0	0.02(0.26)	0.23 FS	0.24 FS
0.7	0	0.19	0.21 FS	0.14 FS
0.5	0.16*	0.21	0.19 FS	0.16 FS
0.3	0.15(0.33)	0.22	0.19 FS	0.14 FS

the early stages because of the low intensity of the peak. The latency displayed by these three systems indicates that initial separation is *via* a mechanism with nucleation-like characteristics rather than spinodal decomposition, which is to be expected considering their close proximity to the metastable region of the phase diagram.

The other systems all display immediate movement of the small angle scattering peak to lower wavevectors, characteristic of phase separation by spinodal decomposition. For the higher volume fraction systems, the exponent given was taken from early times ($t < 16.4\ a^2/D_0$), after which the rate increases continuously. Although the data used was from early times in the simulation, the initial stage of phase separation was rapid at higher volume fractions and low temperatures so the exponents given are descriptive of the intermediate stage or coarsening dynamics.

The phase point dependence of the value of α for systems at $\phi = 0.16$ compares well with previous simulation work on phase separation of alloys, the rate becoming slower as the temperature is decreased due to the slower dynamics of low temperature systems [15]. The value of α also decreased as the volume fraction was increased to $\phi = 0.20$, again reflecting slower coarsening dynamics, in this case due to the increased packing of the particles hindering the restructuring process.

Spinodal decomposition is initiated by long wavelength density fluctuations and the rapid initial stage can be captured well on the simulation timescale. The first key lengthscale to be observed is probably the short lengthscale of the fine interconnected structure. As the temperature decreased the separation process occurred more quickly, leading to an increase in the apparent initial lengthscale. In the more metastable systems, the initial long lengthscale observed results from the long wavelength density fluctuations typical of early time spinodal decomposition, however phase separation is retarded owing to thermal fluctuations. In Figure 10 it can be seen that the characteristic lengthscale at $T = 0.7$ for the $\phi = 0.10$ and 12:6 potential system is smaller than for the higher temperature system of the same volume fraction. This reflects the different initial mechanisms of the phase separation, the system at $T = 0.9$ being more metastable.

The lowest volume fraction system at $\phi = 0.05$ showed quite low values of $\alpha \approx 0.15$ over the temperature range covered in the simulations. The LS exponent of 0.33 is only expected to apply at a relatively late stage when the two phases have reached their near equilibrium proportions would be expected for intermediate stage phase separation. At low volume fractions the incipient clusters are far apart and therefore it takes longer for this state to be achieved. At $T = 0.3$, there is a gradual crossover to $\alpha \approx 0.33$ at later times.

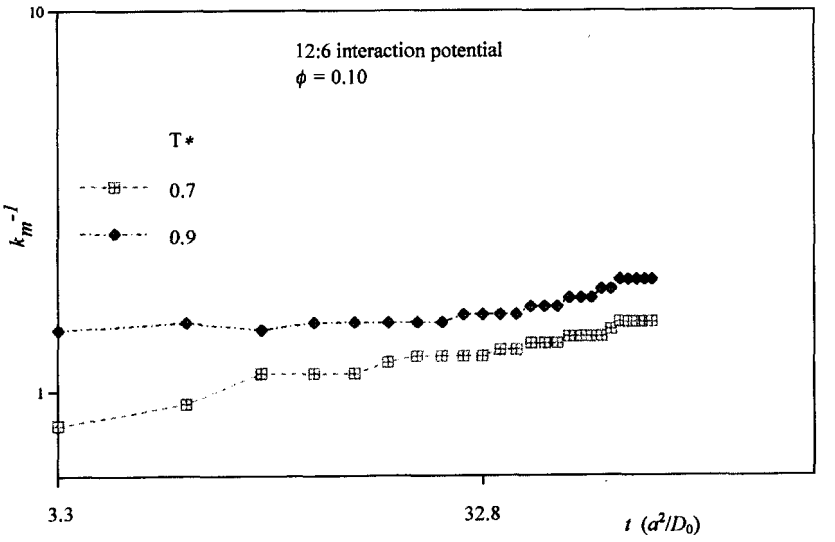

FIGURE 10 Evolution of the characteristic lengthscale, k_m^{-1}, with time for $N = 864$ 12:6 systems at $T = 0.7$ and 0.9 for the volume fraction $\phi = 0.10$.

At $T = 0.5$, the systems interacting *via* the short-ranged 36:18 potentials showed no indication of phase separation, and the longer-ranged 24:12 potential systems only manifested an increase in the characteristic lengthscale after a period of latency. In the systems, with the long-ranged 12:6 potential, phase separation at this temperature was essentially immediate following the quench indicating that they are clearly in the unstable region of the phase diagram.

As a general point, the LS single particle diffusion mechanism is unlikely to be realistic for the longer-ranged potential systems, especially at low temperatures and high volume fractions (although there is a crossover in the $\phi = 0.05$ system at later times). The strong interactions dictate that the rate of coarsening is dependent on cluster–cluster connections rather than on single particle diffusion and the dispersal of small clusters. As the potential becomes shorter-ranged, the particles more easily break away from the clusters, and the particles are then taken up by the larger clusters (*i.e.*, the Ostwald ripening mechanism). The change in the coarsening mechanism is reflected in the increase in coarsening rate as the potential becomes shorter-ranged and the faster LS mechanism takes presidence.

The low temperature behaviour of the inverse of the peak position for the 24:12 potential is shown in Figure 11. Data for volume fractions in the

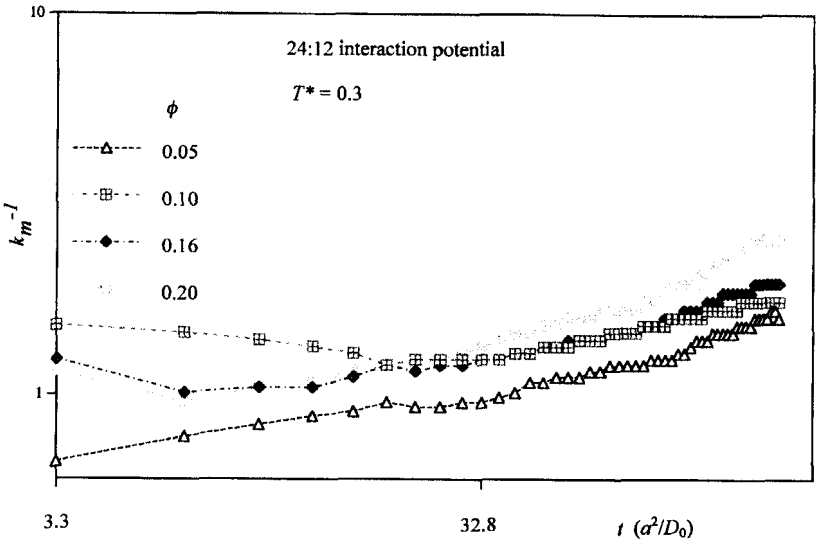

FIGURE 11 Evolution of the characteristic lengthscale, k_m^{-1}, with time for $N = 864$ 24:12 systems at $T = 0.3$ for various volume fractions given on the figure.

range 0.05 and 0.20 are presented in this figure. The early time results are subject to significant noise and it is clear that at the low temperature of $T = 0.3$ that there is progressive growth in the characteristic lengthscale. The exponents for different volume fractions are all similar at $\alpha \approx 0.23$. The highest volume fraction system has a slightly higher exponent of $\alpha \approx 0.26$ and it can be seen from the figure that the characteristic lengthscale in this system is growing faster than for the others. At later times for $\phi = 0.20$, α increased to a value approaching 0.5 as it did in the other systems to a lesser extent, however since the increase was continuous, exponents cannot reliably be extracted from this region. The increase in the value of α suggests the surface tension becomes an important driving force as the separation proceeded and the particles were drawn closer together. The effect of surface tension decreased as the volume fraction decreased, since surface tension driven growth is very much associated with the connectedness of the particles. However for $\phi = 0.05$, the value of α again increased at later times, perhaps due to the increasing influence of the LS mechanism which dominates at low volume fractions.

It can be seen from Figure 11, showing k_m^{-1} with time for the 24:12 potential at $T = 0.3$, that the value of the characteristic lengthscale at later times increases with volume fraction at low temperatures. This implies that the structure of the system is finer and more tenuous at low volume

fractions. The 36:18 potential systems at the same temperature also show movement of the peak to lower wavevectors, as is shown in Figure 12 which covers the same volume fraction range as for Figure 11. The exponent α again decreases with volume fraction, however from the figure it can be seen that the curves at the rates at these intermediate times are very similar. At later times the two higher volume fraction systems show an increase in α to higher values.

The value of the structure factor at a particular wavevector gives a measure of the relative importance of correlations at that wavelength. The intensity of the small angle scattering peak is therefore roughly proportional to the occurrence of the characteristic lengthscale in the system. The peak intensity reflects the extent of phase separation, increasing as both the density difference between the two phases increases and the particles become more ordered in the high density regions. It can be seen from the following results that the phase separation process can continue even if the characteristic lengthscale of the system is not changing.

In the earliest stages of spinodal decomposition, the linearised theory of Cahn and Hilliard predicts an exponential increase in the peak intensity, $S(k_m)$. In this work, the intensity was not found to increase exponentially, even at the earliest times in the slowly evolving short-range potential systems – the time sections over which averages were taken were probably

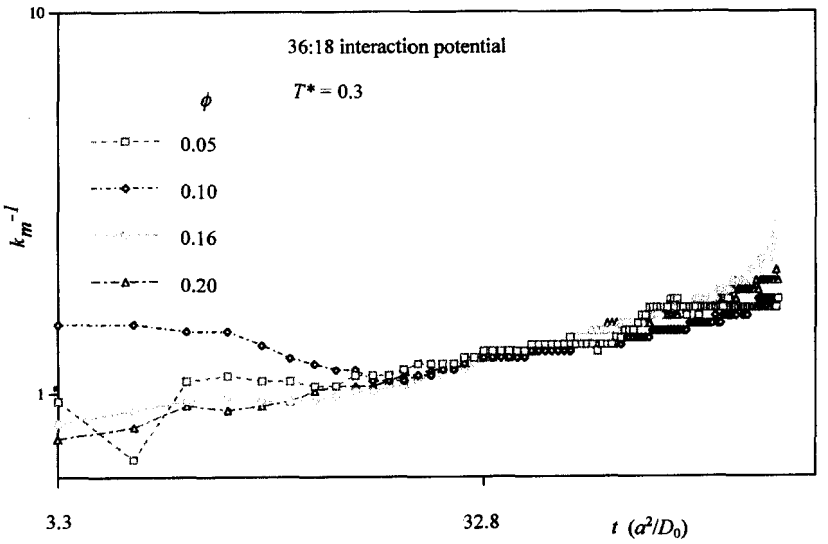

FIGURE 12 As for Figure 11 except the 36:18 potential was used.

too large. Linearised theories are only valid when density fluctuations are very small, which in this work occurs only at early times, often before $t = 3.28\ a^2/D_0$, before the end of the *first* time section. Since there is not enough data to confirm exponential behaviour, the applicability of Cahn and Hilliard's linearised theory to these systems cannot be established. In most systems, the peak intensity was found to increase with a power law dependence with time of the form,

$$S(k_{\max}) \propto t^{\beta} \tag{4}$$

The peak height followed this power law well at all state points in which significant aggregation occurred. The exponent β generally fell in the range 0.8 ± 0.1, which agrees well with previous experimental and computational studies [15, 16].

The peak intensity displayed much less dependence on system size than the peak position. The peak intensity is governed by the importance of the characteristic lengthscale in the system. For the long-range 12:6 potential systems the peak intensity increased immediately after the quench without any signs of latency. The intensity at equivalent times decreased with increasing temperature and decreasing volume fraction, reflecting the position of these systems in the Lennard-Jones phase diagram. Figure 13 shows that in the high temperature systems at $T = 0.9$, power law behaviour is

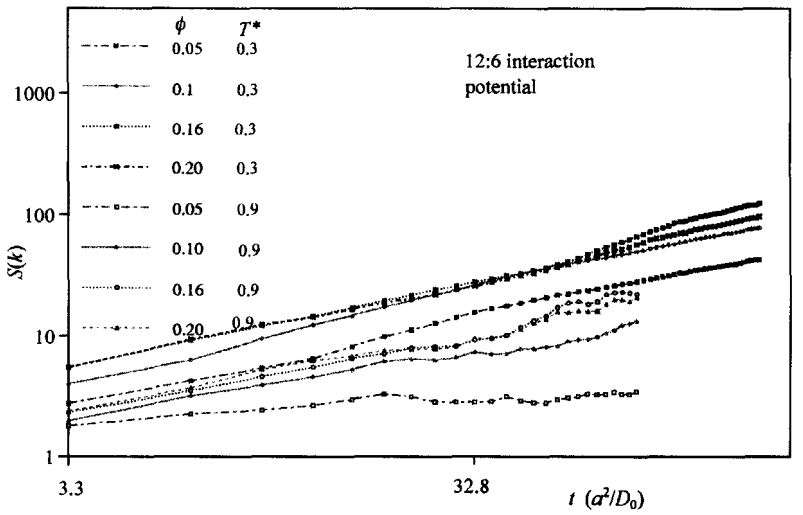

FIGURE 13 The time dependence of the low-k peak height, $S(k_m)$, for a 12:6 system at various volume fractions and $T = 0.3$ and 0.9.

not followed well. The systems at $\phi = 0.05$ and 0.10 at this temperature have low values of β and also show latency in the growth of the characteristic lengthscale. The slow rate of phase separation suggests some degree of metastability at these phase points.

At $T = 0.7$ and $\phi = 0.5$ latency is displayed in the growth of the characteristic lengthscale, however the peak intensity shows behaviour comparable to systems positioned much deeper into the two phase region, as seen in Figure 14. This indicates that although the system is metastable to some extent, there is a significant amount of aggregation of particles. The presence of relatively important thermal motion at this temperature prevents the restructuring which would lead to coarsening of the structure. The value of β (≈ 0.78) also implies a greater rate of phase separation than suggested by the behaviour of the characteristic lengthscale, α. The values given for α, however, were derived from early times before the lengthscale rapidly increased as the clusters filled the finite simulation box. The time dependence of the peak intensity is taken at later times measuring the rate of restructuring in the clusters, which does not seem to be so affected by finite size effects.

Figure 13 shows that the system at $\phi = 0.05$ and $T = 0.3$, crosses to a lower value of β at later times. This corresponds to a crossover to the higher rate in the coarsening exponent, α. The movement of particles from one

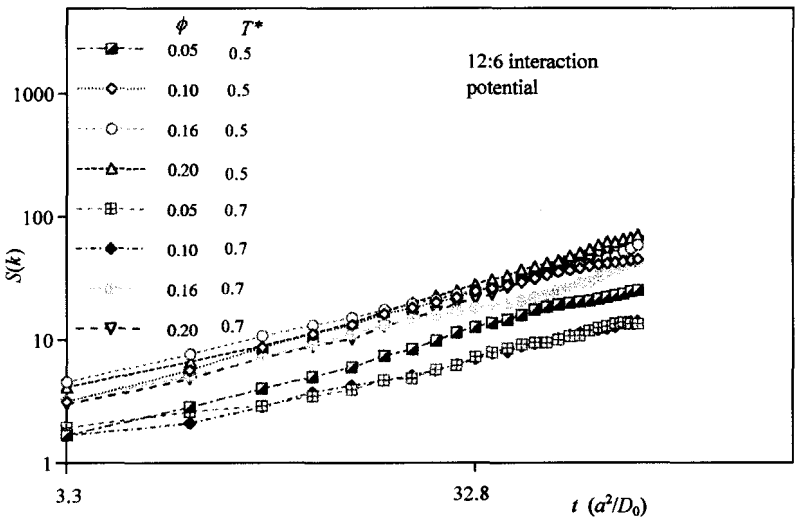

FIGURE 14 The time dependence of the low-k peak height, $S(k_m)$, for a 12:6 system at various volume fractions and $T = 0.5$ and 0.7.

cluster to another such as embodied in the LS coarsening mechanism, may not lead to a large increase in intensity since the decrease in ordering in one cluster will be compensated for by the ordering in another.

The behaviour of the peak intensity is clearly sensitive to the range of the attractive part of the interparticle potential. The intensity of the small angle scattering peak is much lower for the short-range potential systems. The value of β decreases as the potential becomes shorter-ranged for all volume fractions at $T = 0.5$, reflecting the lowering of the two-phase boundary (see Tab. II). The systems close to the two phase boundary (*i.e.*, those with shorter-ranged potentials) have a greater degree of metastability resulting in a slower rate of phase separation.

For all of the systems with the 24:12 potential, the height of the small angle scattering peak increased with time immediately following the quench. There were no indications of latency in the growth of the peak even for the $T = 0.5$ and $\phi = 0.05$ system, which did display position latency. At higher temperatures, the intensity was lower with a slower rate of increase. All of the values for scaling exponent β were lower than expected for spinodal decomposition ($\beta \approx 0.8$), ranging from 0.15 to 0.49, the value increasing with volume fraction. This reflects higher metastability of the high temperature systems, the metastability increasing as the volume fraction decreased and as the systems moved closer to the two phase boundary.

At the higher temperature of $T = 0.5$ for the 36:18 potential, very little evidence was seen of any change in peak intensity with time, these phase points being highly metastable. There was a little overall increase in the intensity indicating a low level of clustering. For the lower temperature systems at $T = 0.3$, the intensity again decreased as the potential became shorter-ranged. The smaller magnitude of the intensity is a result of the slower dynamics leading to a lower extent of phase separation at the same time.

The low temperature systems for the 24:12 potential displayed a strong power law dependence on time with an exponent $\beta \approx 0.7$. It can be seen from Figure 15 that the higher volume fraction examples showed almost identical evolution of the peak intensity. The system at $\phi = 0.05$ also followed the

TABLE II Values of β for the LJ m:n potentials at different volume fractions and at $T = 0.5$. Any different values after a crossover at later times are shown in brackets. The estimated uncertainty is ± 0.05

Interaction potential/ϕ	0.05	0.10	0.16	0.20
12:6	0.75	0.85	0.76	0.93
24:12	0.15	0.29	0.49	0.46
36:18	–	–	–	–

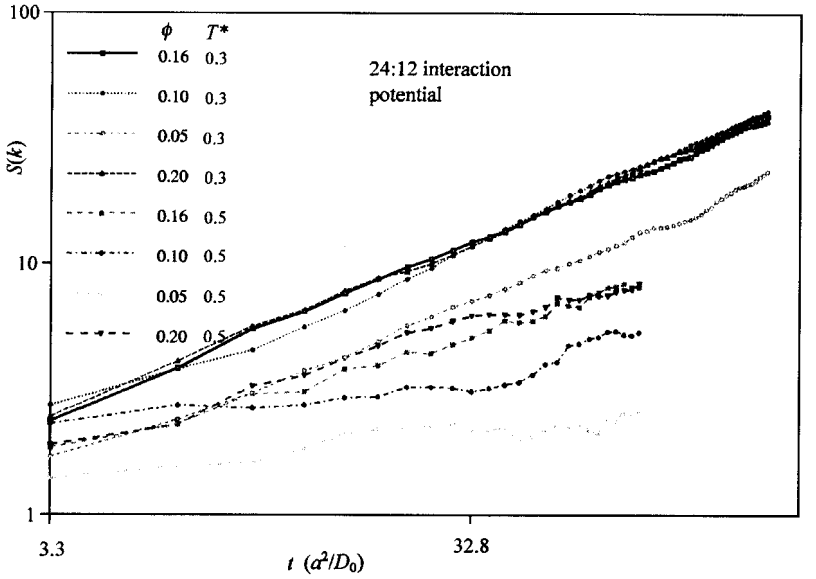

FIGURE 15 The time dependence of the low-k peak height, $S(k_m)$, for a 24:12 system at various volume fractions and $T = 0.3$ and 0.5.

same qualitative time dependence, however the absolute values of the intensity were lower. This was also found from the time dependence of the characteristic lengthscale, suggesting that the mechanism of the separation at $T = 0.3$ was not significantly dependent on the volume fraction.

For the 36:18 interaction potential at $T = 0.3$, the peak intensity displayed good power law time dependence. The intensities for the higher volume fraction systems were similar, falling to lower values for the $\phi = 0.05$ system, as was found in the 24:12 potential systems. The values obtained for β were also very similar at different volume fractions, however for this shorter potential the value of β increased slightly with volume fraction. This was also found for the values of α at these phase points, which characterises the decay of the peak position, reflecting the greater metastability of the lower volume fraction systems.

The plateau region in the characteristic lengthscale found for the 36:18 potential in the $T = 0.3$ and $\phi = 0.05$ system was not echoed by the behaviour of the peak intensity. In fact the exponent β seemed to increase in the plateau regions of the characteristic lengthscale. This could be due to restructuring still taking place even though the characteristic lengthscale was not changing.

3.4. Dynamic Scaling and Scale Invariance

Colloidal systems undergoing spinodal decomposition, in the same way as molecular systems, commonly exhibit dynamic scaling of the structure factor [2, 3, 8, 9, 15, 18–21]. This temporal scaling of the small angle scattering peak occurs when the developing system evolves with the same morphology but on an increasing lengthscale. The general scaling equation is such that if d_f is the fractal dimension of the clusters in the system and $F(k/k_m(t))$ is a time independent scaling function, then a graph of $F(k/k_m(t)) = k_m^{df} S(k/k_m, t)$ against $k/k_m(t)$ is time independent for the period of time over which the dynamic scaling holds and therefore the curves for different times will superimpose.

The original scaling equation, which was proposed for classical spinodal decomposition, uses $d_f = 3.0$ [12, 15]. This scaling can be modified by the use of the fractal dimension of the clusters as the scaling exponent if aggregation proceeds with a fractal morphology [9, 19, 20]. In these cases the value of d_f was observed to decrease from $d_f = 3$ down to lower values of $d_f = 1.7$ with increasing depth of quench [9]. It is therefore clear that the depth of the quench or equivalently the strength of the attraction between the colloidal particles has a strong influence on the values of the fractal dimension.

For any region over which the scaling equation is valid, it is implied that the peak intensity against the peak position should give the fractal dimension of the system, $d_{f(sc)}$, which is the dimension with which the scaling equation will hold,

$$S(k_m, t) \approx k_m^{-d_{f(sc)}}(t) \tag{5}$$

In the initial stages of phase separation, especially if there is some degree of latency in the evolution, a fractal dimension will not be found by this method. Also during any crossover in rates, or in the final stages when the peak position has collapsed to zero, this method will not yield a fractal dimension for the system and dynamic scaling is not valid. The absence of a dynamic self-similarity in the structure factor, however, does not prove the absence of any fractal structure in the system. For example a changing fractal dimension as a result of restructuring may not be detected by this method. In addition, the lengthscale of the peak maximum will not distinguish any surface fractal structure, as determined from an analysis of the pair distribution functions.

Many of the simulated systems showed well-defined power law regions in the plots of $S(k_m)/k_m$, indicating that the structure was evolving in a

self-similar manner with time. The values of $d_{f(sc)}$ were generally quite high though, falling between 2.0 and 3.0. A decrease to very low values of $d_{f(sc)}$, occasionally seen at later times in the high volume fraction systems, is probably due to the slowing of the rate of increase in peak intensity due to the approach of the densities of the two phases to near equilibrium values, while the peak position was still decreasing due to restructuring. Therefore it does not necessarily imply the formation of structures with these low fractal dimensions.

The long-ranged 12:6 potential systems generally exhibited a steep initial power law dependence of peak intensity on peak position, which decreased at later times for the higher volume fractions. For the more metastable phase points, $\phi = 0.05$ at $T = 0.9$ and 0.7, there was no power law relationship, as expected since there was no significant growth in characteristic lengthscale. The higher volume fractions at $T = 0.9$ did display a power law dependence giving an exponent of 2.1 for $\phi = 0.10$ and 2.3 for $\phi = 0.16$, suggesting that the clusters at high temperatures were more diffuse.

At temperatures of $T = 0.7$ and 0.5, all the systems displaying power law behaviour gave a very high initial exponent of $d_{f(sc)} > 3.0$, as seen in Figure 16. This reflects the large influence of restructuring in these long-ranged potential systems, the densification of the growing clusters caused an

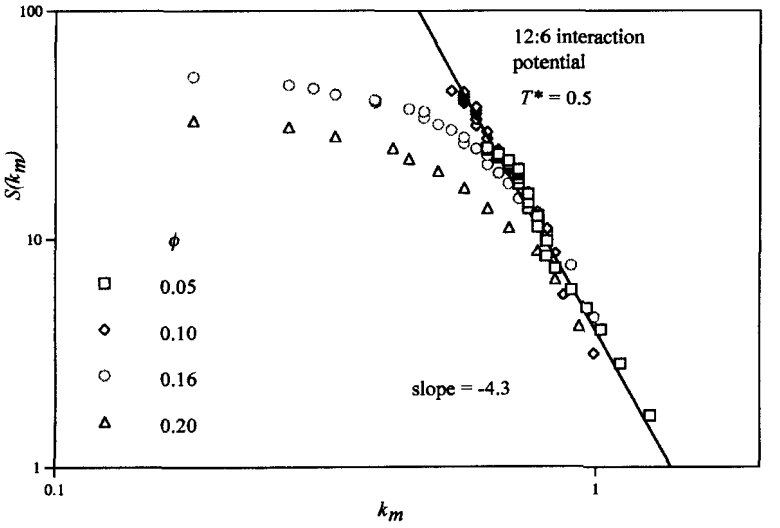

FIGURE 16 The dependence of the low-k peak height, $S(k_m)$, *vs.* k_m for a 12:6 system at various volume fractions and $T = 0.5$.

increase in intensity of the peak at a much faster rate than the increase in lengthscale. This highlights the problem in associating the scaling exponent with the fractal dimension of the system if restructuring was occurring. If restructuring is strong, the structure of the centre of the cluster could be very different to that at the edge of the cluster, but the scaling exponent would give an average value of the two which may be misleading if used to interpret the evolving structure.

At later times in the high volume fraction systems, the exponent decreased to much lower values of $d_{f(sc)} \approx 1.6$. This does not necessarily indicate the formation of very diffuse fractal clusters. It is more likely to be a reflection of the rapid collapse of the small angle scattering peak to zero, an effect that is exacerbated by the finite size of the simulation cell.

The low temperature behaviour of $S(k_m)/k_m$ is shown in Figure 17. At $T = 0.3$, the low temperature slows down restructuring to some extent due to the reduced magnitude of the random displacements. This leads to lower initial values of the scaling exponent of ≈ 3, the value expected for classical spinodal decomposition. In the highest volume fraction system, $\phi = 0.20$, where the particles are more closely packed the rearrangement occurs relatively quickly. In this system the exponent is ≈ 4 which is still a little higher than expected.

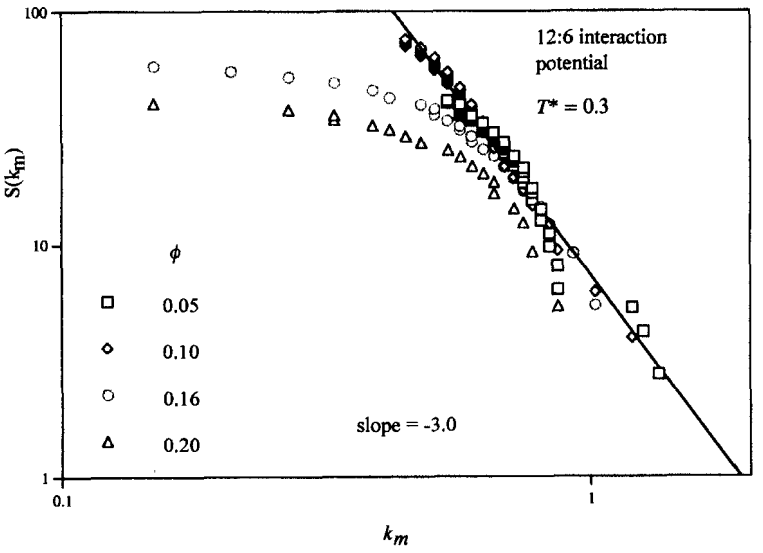

FIGURE 17 The dependence of the low-k peak height, $S(k_m)$, *vs.* k_m for a 12:6 system at various volume fractions and $T = 0.3$.

The values of $d_{f(sc)}$ for the three potential systems at $T = 0.3$ are given in Table III. The high temperature systems ($T = 0.5$) for the 24:12 potential show little development of the peak intensity and this is reflected in the relationship between the peak intensity and the peak position of these systems. At the lowest volume fraction, the system shows little evidence of any phase separation or peak development. At the three higher volume fractions, although there was some phase separation, there was no clear power law relationship and a value for the exponent was not estimated. Since the high temperature systems of particles interacting with the relatively short-ranged 36:18 interaction potential did not show any significant phase separation, power law dependence between the peak height and the peak position was not expected or found at any volume fraction.

The lower temperature systems, $T = 0.3$ for the 36:18 potential all displayed an initial exponent of $d_{f(sc)} \approx 3$. At $\phi = 0.05$ and $T = 0.3$, the peak position froze at later times. The exponent at earlier times (before the arrest of change in the peak position) was high at $d_{f(sc)} \approx 3$, indicating that the although the structure was self-similar before the characteristic length scale set in, it was unlikely that it had a fractal structure. The system with the highest volume fraction, $\phi = 0.20$, evolved with $d_{f(sc)} \approx 3$, for nearly the entire simulation. At volume fractions $\phi = 0.10$ and 0.16, a crossover to lower values of $d_{f(sc)}$ occurred at later times. The lower volume fraction system crossed to the lowest value of $d_{f(sc)}$ as expected since at higher volume fractions the particles are more tightly packed.

The behaviour of the peak height and the peak position had less dependence on the interaction potential as the volume fraction increased. The highest volume fraction systems followed an almost identical line with an exponent $d_{f(sc)} \approx 3$, demonstrating the relative unimportance of the attractive potential range when the particles are closely packed at high densities. The high exponent indicates a self-similar but compact structural evolution with time. A fractal structure would not be expected in these dense systems. The long-range potential system had a little higher initial exponent and displayed more curvature to lower exponents at longer times. In longer-ranged potential systems, rearrangement was significant from the

TABLE III Values of $d_{f(sc)}$ for different potentials at $T = 0.3$ and different volume fractions. Any different values after a crossover at later times are shown in brackets. The accuracy of the values given is estimated to be ± 0.1

Interaction potential/ϕ	0.05	0.10	0.16	0.20
12:6	2.9	3.1	2.9(1.7)	4.0(1.6)
24:12	3.0(2.2)	3.0	3.0(1.9)	3.0(1.1)
36:18	3.0(0)	3.0(1.9)	3.0(2.3)	3.0(2.9)

start of the simulation causing the higher initial value for the exponent. Phase separation also occurred more quickly overall and therefore the small angle scattering peak quickly collapsed to zero as the cluster filled the simulation box which affected the evolution of the peak position and therefore the calculated value of $d_{f(sc)}$.

At $\phi = 0.16$, the two longest-ranged potential systems again had similar power law behaviour giving an exponent $d_{f(sc)} \approx 3$. The 36:18 potential however had a lower exponent of ≈ 2.3, suggesting that there was less restructuring for this potential allowing fractal structures to persist for longer times. The long-range 12:6 potential showed curvature at late times due to the faster rate of phase separation and the influence of finite size effects. The 24:12 system did not display this curvature, the shorter-range potential leading to slower phase separation.

The shorter-ranged potential systems were more affected by noise at early times due to the lower peak intensity. For the 24:12 potential at low temperatures similar power law dependence is found initially at all volume fractions with an exponent of ≈ 3. At $\phi = 0.1$, the same exponent also characterises the separation at later times. For all other volume fractions a crossover to lower exponents occurred as time evolved. The lowest volume fraction system, $\phi = 0.05$, displays the smallest value for the exponent, indicating the formation of less compact clusters. The two highest volume fraction systems both crossed over to a smaller value for the exponent at later times, the exponent becoming smaller at higher volume fractions. In these cases the decrease in exponent was probably due to the rapid collapse of the peak to zero, caused by the finite size of the simulation box.

Dynamic scaling of the small angle scattering peak was attempted using the calculated values of $d_{f(sc)}$ obtained from the plots of $S(k_m)/k_m$. Dynamic scaling was, however, found to be quite insensitive to the exact value of $d_{f(sc)}$. In many cases scaling could be produced using a fairly wide range of values of $d_{f(sc)}$ (± 0.2). Most of the systems that were thought to be in the spinodal region exhibited dynamic scaling at intermediate times. The scaling exponents were typically high, $\approx 3.0 \pm 0.2$, suggesting that the aggregates forming do not have a fractal structure. Instead the clusters had a compact smooth structure. Scaling of the peak maximum could also often be found using the very low exponents at later times for the high volume fractions from the $S(k_m)/k_m$ plots, however in these cases the shape of the whole peak did not scale well.

Scaling is only expected when the phase separation is in a coarsening regime. There will not be scaling of the small angle scattering peak in the initial stages of separation, in crossover regions or when the peak has

collapsed to zero at late times. There is usually some deviation from the expected scaling near to the peak at $k = 1$ which suggests some variance in the characteristic length for these relatively small systems. Even in experimental systems, the fractal dimension is an average over the whole system so some degree of uncertainty in the scaling is to be expected.

For systems with the long-ranged 12–6 potential, scaling was not observed at high temperatures for low volume fractions; the phase points displayed signs of metastability. Scaling was also not observed after deep quenches at high volume fractions, except at very early times. In these systems, phase separation was rapid and clusters quickly filled the simulation box, causing the collapse of the small angle scattering peak to zero. The crossover to low values of $d_{f(sc)}$ seen in the high volume fraction $S(k_m)/k_m$ plots was not reflected by the dynamic scaling. Again these lower values of $d_{f(sc)}$ as calculated by $S(k_m)/k_m$ scaled the peak maximum, however the overall shape of the peak was not invariant with time. This suggests that significant changes in the cluster morphology and consequently the occurrence of different length-scales occurred at later times at high volume fractions.

At the lower volume fractions phase separation was slower enabling scaling to be observed. The exponent with which dynamic scaling occurred was generally ≈ 3, which was lower than the value of $d_{f(sc)}$ taken from the $S(k_m)/k_m$ plots. The high values of $d_{f(sc)} \approx 4$ obtained from these plots often scales the peak maximum well, but for the best overall scaling of the peak shape the lower value of ≈ 3 was better.

Dynamic scaling with an exponent $d_f = 3.0$ has been seen in experiments on transient gelation of colloidal systems with much shorter ranging attractive potentials for small quenches [3]. In these experimental systems, d_f was observed to decrease to a value of $d_f = 1.7$ with increasing quench depth [3]. For the 12:6 potential in this simulation work, the low volume fraction system, $\phi = 0.05$, at $T = 0.3$ did scale with a lower exponent of $d_f = 1.7$ at later times (see Fig. 18). An estimate of the value of d_f was not taken at this time from the plots of $S(k_m)/k_m$, since the line has no clear straight region.

The applicability of the phenomenological equations of Furukawa was also tested. The form of the scaling function $F(k/k_m)$ given by Furukawa, has been found to give a reasonable representation of the behaviour of aggregating colloids from light scattering results and of molecular dynamics simulations of aggregation of LJ particles. This function for an 'off-critical' density quench is,

$$\tilde{F}(k/k_m) = \frac{3(k/k_m)^2}{2 + (k/k_m)^6} \tag{6}$$

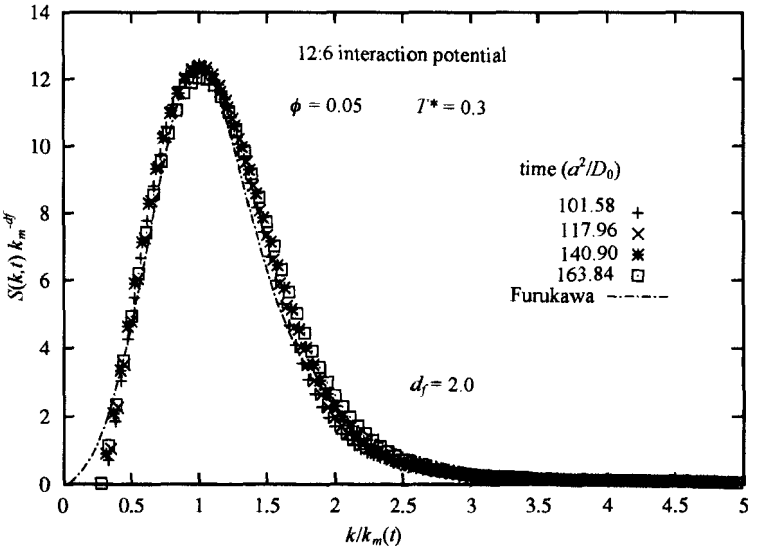

FIGURE 18 Demonstration of the scaling of the low-k peak of the structure factor for 12:6 and $N = 864$ systems. The approximate formula by Furukawa from Eq. (6) is also shown. $\phi = 0.05$ and $T = 0.3$.

In general the form given by Furukawa was found to agree well with the simulation results at low volume fraction, however at higher volume fractions or at late times there are significant deviations. The validity of the equations relies on the clusters being well defined, an assumption fulfilled best at low volume fractions.

The low volume fraction systems were well approximated by the form given by Furukawa. As the volume fraction increases the peak tends to become wider and the fit is less appropriate (see Fig. 19) since at high volume fractions clusters are not well defined which is a necessary approximation for the theory of Furukawa.

An estimate of the fractal dimension of the aggregating systems can also be obtained from the high wavevector side of the small angle scattering peak [33],

$$S(k) \propto k^{-2d_f+d_s} \tag{7}$$

where d_s is the so-called surface dimension. For a fractal aggregate, $d_s = d_f$ and the slope of a log–log plot of $S(k)$ *vs.* k is therefore $-d_f$ and for scattering from smooth surfaces (with $d_s = 2$ and $d_f = 3$) the slope is -4. A rough fractal surface surrounding a compact core will give a slope between

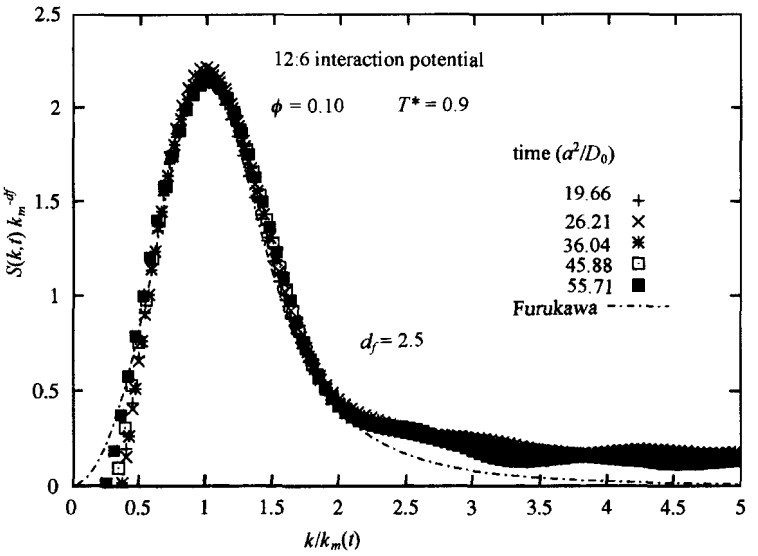

FIGURE 19 Demonstration of the scaling of the low-k peak of the structure factor for 12:6 and $N = 864$ systems at $\phi = 0.10$ and $T = 0.9$. The approximate formula by Furukawa from Eq. (6) is also shown.

-3 and -4 [19]. The systems in this work displayed predominantly a slope of ca. -4, indicating smooth surfaces surrounding a dense cluster, especially at later times. As with the other methods for calculating d_f, the only clear indications of a low dimensional structure were either early in the phase separation or at high temperatures and low volume fractions (the systems that separate more slowly). Even in these cases the dimension was still typically high at ca. 2.5 and the structure can therefore only be considered to be marginally fractal.

Evidence of a low initial fractal dimension is not found in this work for the long-ranged potentials or in the low temperature, high volume fraction systems. Restructuring rapidly led to the formation of much denser clusters, especially for longer-ranged potentials, as revealed by the short-range structure in the pair distribution functions.

4. CONCLUSIONS

A Brownian Dynamics computer model was used to investigate the phase separation characteristics of a homogeneous distribution of model attractive monodisperse colloidal particles following on from a quench into the

vapour – liquid or vapour – solid parts of their phase diagrams. Simulations were carried out with Lennard-Jones type 12:6, 24:12 and 36:18 potentials, which have increasingly shorter ranged attractive parts to the potentials along this series.

This study has been able to establish the sensitivity to the potential type of the phase-separation behaviour of fluids into a low density (gas-like) and high-density liquid or solid-like states. A number of trends have emerged. The morphology during the phase-separation was quite sensitive to the width of the potential well – even in the relatively narrow range probed in this study (much less than can be covered in experimental colloidal systems). The morphology was also dependent on the particle number density and temperature. It is quite a complex multiparameter issue, which we have only been able to make a partial exploration of in this study. To characterise this behaviour in terms of a few universal 'exponents' is missing many of the subtleties and thermodynamic influences. The local crystal-like ordering observed in the denser regions of the inhomogeneous mixture during phase separation is a pheneomenon that could be more widespread than colloidal systems. Similar 'local' crystallisation during spinodal decomposition could also take place in a wide range of material mixtures such as alloys and polymer blends in the immiscibility gap.

Characterisation of aggregate structure in systems without permanent bonds by fractal measurements is difficult. Due to the large influence of restructuring, the structure is continually changing both with time and with the exact region of aggregate being observed. The value of the dimension obtained therefore highly dependent on the lengthscale that is probed by the characterisation technique.

Acknowledgements

JFML thanks the Engineering and Physical Sciences Research Council of Great Britain (EPSRC) for the provision of a research studentship. DMH thanks the EPSRC for funding DIGITAL AlphaStations with which this work was carried out.

References

[1] Heyes, D. M., Nuevo, M. J. and Morales, J. J. (1998). "Translational and rotational diffusion of dilute solid amorphous spherical nanocolloids by molecular dynamics simulation", *Molec. Phys.*, **39**, 985.

[2] Verhaegh, N. A. M., Asnaghi, D., Lekkerkerker, H. N. W., Giglio, M. and Cipelletti, L. (1997). "Transient gelation by spinodal decomposition in colloid-polymer mixtures", *Physica A*, **242**, 104.

[3] Verhaegh, N. A. M., van Duijneveldt, J. S., Dhont, J. K. G. and Lekkerkerker, H. N. W. (1996). "Fluid–fluid phase-separation in colloid-polymer mixtures studied with small-angle light-scattering and light microscopy", *Physica A*, **230**, 409.
[4] Lodge, J. F. M. and Heyes, D. M. (1998). "Structural evolution of phase-separating model colloidal liquids by Brownian dynamics computer simulation", *J. Chem. Phys.*, **109**, 7567.
[5] Lodge, J. F. M. and Heyes, D. M. (1999). "Rheology of transient colloidal gels by Brownian dynamics computer simulation", *J. Rheol.*, **43**, 219.
[6] Vliegenthart, G. A., Lodge, J. F. M. and Lekkerkerker, H. N. W. (1999). "Strong weak and metastable Liquids: Structural and dynamical aspects of the liquid state", *Physica A*, **263**, 378.
[7] Heyes, D. M. (1997). The Liquid State: Applications of Molecular Simulations, J. Wiley & Sons, Chichester.
[8] Ermak, D. L. (1975). "A computer simulation of charged particles in solution. I. Technique and equilibrium properties", *J. Chem. Phys.*, **62**, 4189.
[9] Poon, W. C. K., Pirie, A. D. and Pusey, P. N. (1995). "Gelation in colloid-polymer mixtures", *Faraday Discuss.*, **101**, 65.
[10] Grant, M. and Elder, K. R. (1999). "Spinodal decomposition in fluids", *Phys. Rev. Lett.*, **82**, 14.
[11] Lifshitz, I. M. and Slyozov, V. V. (1961). *J. Phys. Chem. Solids*, **19**, 35.
[12] Binder, K. (1987). "Theory of First Order Phase Transitions", *Rep. Prog. Phys.*, **50**, 783.
[13] Binder, K. and Stauffer, D. (1974). "Theory for the Slowing Down of the Relaxation and Spinodal Decomposition of Binary Mixtures", *Phys. Rev. Lett.*, **33**, 1006.
[14] Siggia, E. D. (1979). "Late Stages of Spinodal Decomposition in Binary Mixtures", *Phys. Rev. A*, **20**, 595.
[15] Furukawa, H. (1985). "A dynamic scaling assumption for phase-separation", *Adv. Phys.*, **34**, 703.
[16] Carpineti, M. and Giglio, M. (1992). "Spinodal-type dynamics in Fractal Aggregation of Colloidal Clusters", *Phys. Rev. Lett.*, **68**, 3327.
[17] Asnaghi, D., Carpineti, M., Giglio, M. and Vailati, A. (1995). "Light scattering studies of Aggregation Phenomena", *Physica A*, **213**, 148.
[18] Gunton, J. D., San Miguel, M. and Sahni, P. S., In: '*Phase Transitions and Critical Phenomena*', Eds., Domb, C. and Lebowitz, J. L. (Academic Press, London, 1983), Vol. 8, Ch. 3.
[19] Haw, M. D., Sievwright, M., Poon, W. C. K. and Pusey, P. N. (1995). "Structure and Characteristic length scales in Cluster-Cluster Aggregation", *Physica A*, **217**, 231.
[20] Butler, B. D., Hanley, H. J. M., Hansen, D. and Evans, D. J. (1995). "Dynamic scaling in an aggregating 2D Lennard-Jones system", *Phys. Rev. Lett.*, **74**, 4468–4471.
[21] Butler, B. D., Hanley, H. J. M., Hansen, D. and Evans, D. J. (1996). "Aggregation of a quenched Lennard-Jones system under shear", *Phys. Rev. B*, **53**, 2450–2459.